Impact of Substrate and Processing on Confinement of Nafion Thin Films

*Ahmet Kusoglu, Douglas Kushner, Devproshad K. Paul, Kunal Karan, Michael A. Hickner, and Adam Z. Weber**

Thin films of ion-conducting polymers are an important area of study due to their function in many electrochemical devices and as analogues for interfacial phenomena that occur in bulk films. In this paper, the properties of Nafion, a prototypical ionomer, are investigated as thin films (4 to 300 nm) on carbon, gold, and platinum substrates that are fabricated using different casting methods and thermal histories. Specifically, water uptake, swelling, and morphology are investigated by quartz-crystal microbalance, ellipsometry, and grazing-incidence X-ray scattering to develop structure/property/processing relationships. For all substrates, as the films' thickness decreased, there is an initial decrease in swelling followed by a subsequent increase for film thicknesses below ≈20 nm due to a disordering of the film hydrophilic/hydrophobic structure. Decreased swelling and less structural order is observed on gold for spin-cast films compared to self-assembled films; the opposite effect is observed for films on carbon. The presented systematic data set and analyses represent a thorough study of the behavior of Nafion thin films on model substrates of interest in metal catalyst/carbon electrodes, and these insights help to elucidate the underlying polymer physics and confinement effects in these and related systems.

1. Introduction

Research activities in energy generation, conversion, and storage have dramatically increased due to the need for a sustainable energy infrastructure. Technologies including fuel cells, redox flow batteries, and solar-fuel generators represent promising options as their combination can result in clean and sustainable stationary and transportation energy solutions. These electrochemical devices involve multiple functional layers and combinations of materials with varying physical processes such as ion conduction, multiphase fluid flow, chemical reactions, and generally require the transport of charged intermediates (e.g., protons, hydroxide anions, redox cations) through a solid-state ion-conducting polymer membrane or ionomer and into inorganic catalytic inclusions where redox reactions occur.[1] Transport across these hybrid polymer/inorganic interfaces is crucial for the operation of the devices, in particular in fuel-cell catalyst layers[2–4] or vapor-fed solar-fuel devices,[5] where ion conduction occurs through and along ionomer thin films covering the catalytic sites.[6] The structure of ion-conducting polymers when confined to a thin film can be influenced significantly, resulting in drastically different transport characteristics compared to the behavior of bulk membranes.[7,8] Thus, the presence of ionomers as a thin film in fuel-cell catalyst layers could explain the observed transport limitations therein, where reduced water uptake[9] and depressed proton conductivity[10] have been observed. Moreover, there is very little direct measurement of the properties of these thin films and more detailed investigations are warranted to understand their function in devices.

Perfluorinated sulfonic-acid (PFSA) ionomers, such as Nafion membrane, are the most widely used materials for electrochemical applications requiring a proton-conducting polymer. Nafion's chemical structure is comprised of a perfluorinated backbone that provides both mechanical and chemical stability, and randomly placed tethered perfluoroether side chains terminated with sulfonic acid groups, which impart its remarkable proton-conduction capabilities.[11–14] The structure of Nafion in bulk membranes (5 to 200's μm thick) has been extensively studied using both small- and wide-angle X-ray and neutron-scattering techniques, and microscopy.[11,15–23] Typical scattering profiles and real-space images of Nafion demonstrate a phase-separated morphology, which is comprised of semi-periodic ionic domains with a scattering maximum at q = 1 to 2 nm^{-1} (referred to as the ionomer or water peak), and a semi-crystalline matrix contributing to a broad scattering peak at lower q-values (0.3 to 0.5 nm^{-1}) arising from inter-crystallite spacing.[11,15–20,24] The structure in these membranes is predominantly dominated by the bulk material, as the

Dr. A. Kusoglu, Dr. A. Z. Weber
Environmental Energy Technologies Division
Lawrence Berkeley National Laboratory
Berkeley, CA 94720, USA
E-mail: azweber@lbl.gov
D. Kushner, Prof. M. A. Hickner
Department of Materials Science and Engineering
The Pennsylvania State University
University Park, PA 16802, USA
D. K. Paul, Prof. K. Karan
Department of Chemical Engineering
Queen's University
Kingston, Ontario K7L 3N6, Canada

DOI: 10.1002/adfm.201304311

near-interface regions do not account for a significant volume fraction of the system. Furthermore, Nafion's ionic domains can absorb up to 15 and 22 water molecules per sulfonic acid group when equilibrated in saturated vapor or liquid water, respectively,[11,18,22,25–27] and the ionic conductivity of the material is significantly affected by the water content.[11,13,14,18,28] Although the structure and transport characteristics of Nafion membranes have been described in depth in the literature,[3,11–14,16,18,26,28–32] the behavior of this material when confined to a thin-film morphology is still not well understood.

Thin-film confinement is known to affect the phase behavior of uncharged block-copolymer systems.[33] In thin films, surface interactions and confinement to thicknesses that approach the characteristic domain size of the copolymers can cause anisotropy in the orientation of domains and pose significant limitations to self-assembly, resulting in morphologies that differ from the analogous bulk materials. Ionomers are more complex than many widely studies polymers due to the presence of electrostatic interactions, hydrogen bonding, and less well-defined chain structure, but their self-assembly is expected to be influenced by wetting interactions at both the substrate and free (vapor) interfaces as well as by topological confinement effects.

Recent studies on ionomer thin films have demonstrated that confinement as well as variations in substrate wetting interactions result in differences in orientations of ionic domains that could limit water uptake.[34–37] Moreover, mass transport at the bulk membrane interface was shown to correlate with the fractional area accessible for water entry through the surface ionic domains,[22] and thus wetting and sorption interactions at interfaces could aid in understanding transport mechanisms in bulk membranes as well. Also, the structure at the top interface of films can result in different ionomer wetting and hydrophilicity in the presence of saturated vapor or liquid water.[21,35,38] All of these morphological and surface effects can help to explain the observed limitations in water uptake, mobility and permeability [4,36,37,39] as well as decreased ionic conductivity and increased ion-conduction activation energy[8,40,41] when Nafion is topologically confined. To further complicate developing deeper understanding of these materials, our recent studies have shown that in thin films of less than 50 nm in thickness, water uptake may increase in self-assembled films due to limited phase separation between hydrophilic and hydrophobic domains and decreased hydrophobic-domain elastic forces, which prevent dissolution of the ionomer.[8]

Most of the work on Nafion thin films has occurred on silicon substrates, which, although of interest for solar-fuels applications, is not of practical interest for many other electrode applications where precious metals or carbon are typically used as catalytic substrates. On silicon, Nafion films with thicknesses of less than 25 to 50 nm exhibit negligible scattering without a strong ionomer peak in grazing-incidence small-angle X-ray scattering (GISAXS) experiments, while showing more mixing of smaller hydrophobic and ionic domains as observed by TEM,[8] implying a change in phase-separation behavior with thickness. Another evidence of the change of the film internal and surface morphologies with film thickness was observed by surface wettability wherein the sub-50 nm thick films exhibited a hydrophilic surface whereas thicker films showed a hydrophobic surface.[42] Also, a recent neutron reflectivity study suggested that domains could be oriented parallel to the substrate at the Si wafer interface.[43] However, whether this phenomenon is specific to silicon or controlled by non-specific film\substrate topological interactions that are processing dependent remains to be answered. Moreover, annealing and/or pretreatment of bulk Nafion membrane changes its water uptake and transport properties due to changes in membrane morphology and semicrystallinity.[17,18,20,25,32] Annealing induces more crystalline order in the membrane thereby limiting the water uptake, which influences the material's mechanical and transport properties. Therefore, it is of interest to explore the role of annealing in the confinement-driven changes in structure and water uptake of thin films. Similarly, not only the thermal history but also the processing method for casting thin films may result in different behavior and is relevant for typical thin films in porous electrodes.

This work systematically analyzes the effect of confinement on the structure\function relationships and water uptake in Nafion thin films under different processing conditions on gold, carbon, and platinum substrates. Specifically, impacts of annealing, casting method (spin cast versus self assembly), and substrate type were studied in terms of the film morphology using GISAXS, mass gain with quartz crystal microbalance (QCM), and swelling using ellipsometry.

2. Results and Discussion

This study focuses on a series of Nafion films with thicknesses ranging from 4 to 300 nm. Within this film-thickness range, confinement effects are expected to have a significant impact on the structure and properties of the ionomer, in particular as the film thickness approaches the size of crystallites (≈20 nm), the hydrated domains (3 to 6 nm), or the reported diameter (3 to 5 nm) of rod-like colloids of Nafion in solution.[16–18,20,24,44] Furthermore, the characteristics observed for films of less than 10 nm are relevant for understanding these functional materials' properties in porous electrodes where the ionomer exists as a very thin film covering the catalyst particles.[6,14,45]

2.1. Morphology

As phase-separated polymer films become thinner, one expects that the morphology will change from being isotropic or reflective of the bulk membrane to a structure that is dependent on the substrate/ionomer interactions which become dominant for thin samples. In fact, as observed with silicon substrates, the substrate polarity impacts thin-film morphology below ≈100 nm in film thickness.[34] Furthermore, as the films begin to approach 50 nm or less, the structural features become more difficult to distinguish using scattering and microscopy, which is an indication of mixing of the hydrophilic and hydrophobic domains.[8] **Figure 1** summarizes the GISAXS profiles for the different substrates explored in this paper, namely, carbon, platinum, and gold, and for different polymer film thicknesses at 100% RH (see Figure S4, Supporting Information, for the patterns of unannealed carbon). From the figure, it is readily

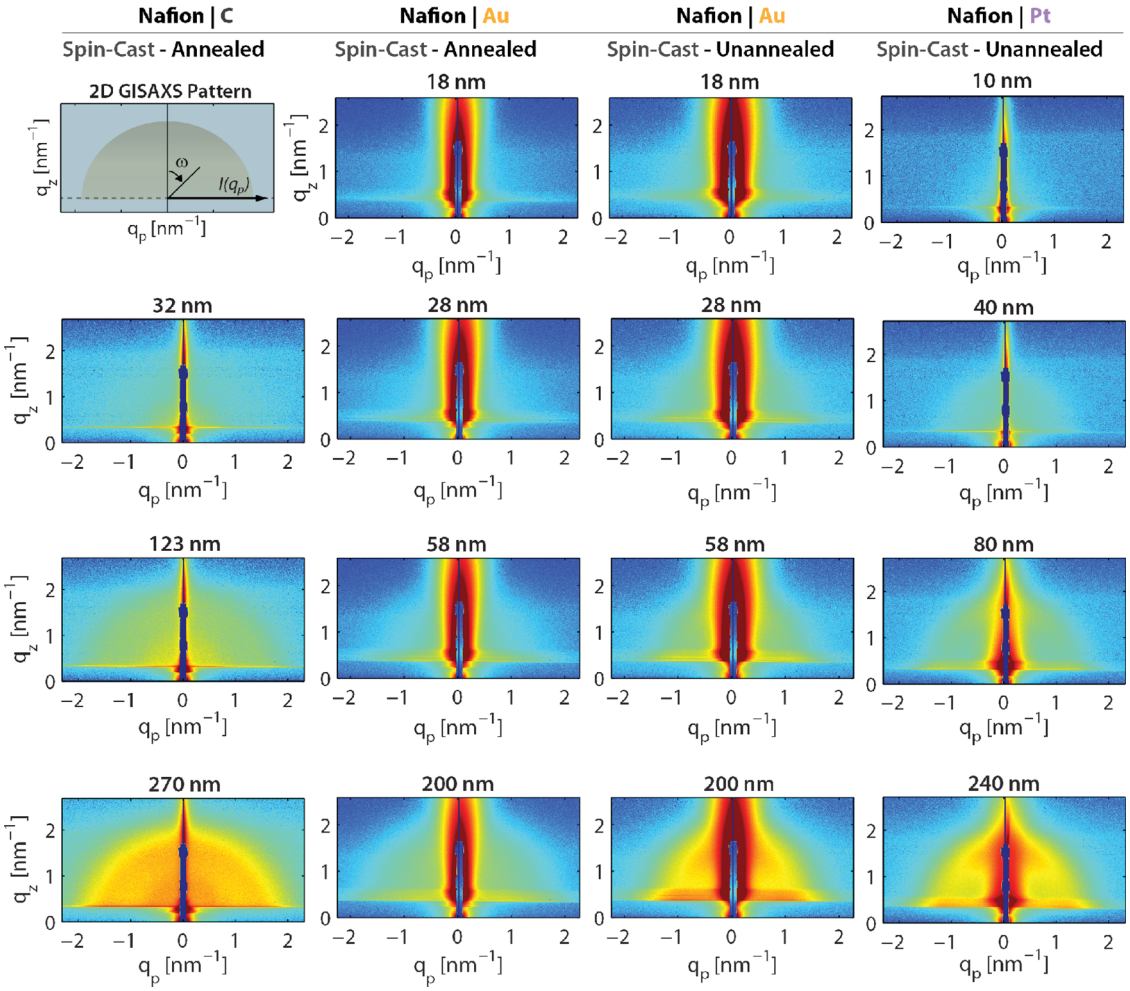

Figure 1. 2D GISAXS patterns for vapor-saturated (100% RH) Nafion films of various thicknesses spin-cast on carbon (C) (annealed), gold (Au) (annealed and unannealed), and platinum (Pt) (unannealed) substrates. Color scale representing the intensity (I) is the same for each substrate. The schematic (top, left) depicts how line cuts are taken for I-q_p profiles parallel to the substrate and orientation is defined for I-ω profiles in the following figures.

apparent that, similar to the analysis on silicon, the thinner-films' structure becomes less distinct in that the scattering ring associated with the ionic domains becomes more difficult to distinguish at thicknesses below approximately 20 nm. It should be noted that the dry patterns demonstrated no observable scattering peak except for the thickest films (see Figure S2, Supporting Information). Comparisons of the substrates seem to indicate a more well-defined and semicircular ionomer peak on carbon than on gold and platinum for nominally the same thickness. This trend with polymer order that depends on substrate composition may be due to the way the polymer interacts with the substrate surface, thereby implying that substrate/film interactions influence the structural order, for example, the size distribution of the polar domains.

Comparisons of line profiles parallel to the substrate, I(q_p), shown in **Figure 2**a reveal that the peak for the sample on carbon is broader than for samples on gold and platinum, with the platinum-supported sample having the most well-defined peak among the samples with the same heat treatment.

The peak is shifted to a higher q value on carbon, thereby indicating smaller domains, which is especially pronounced for the annealed films that were heat treated at 146 °C for 60 min. In addition, the existence of the crystallite-spacing peak at q = 0.55 nm^{-1} in the annealed sample also seems to suggest that the annealing process induced some crystallinity in the film samples on carbon, which may be indicative of weaker surface interactions since the annealed gold samples do not exhibit such a peak (although a similar peak was witnessed for Nafion on a silicon substrate,[34] see Figure S6, Supporting Information). It should be noted that the dry sample patterns demonstrated no noticeable scattering except for the thickest films (see Figure S2, Supporting Information). As seen in Figure 2b, the films on gold, and to a slightly lesser extent on platinum, display very anisotropic behavior. This is not unexpected as one expects stronger interactions of the sulfonic acid and sulfur-containing moieties (e.g., thiols) with the metal substrates than with carbon.[46] This anisotropy in terms of scattering-angle dependence is also similar to that seen with hydrophobized (n-octyltrichlorosilane passivated) silicon surfaces.[34] It also appears that Nafion interactions with gold and platinum may induce ordering of the Nafion near the substrate interface. From Figure 1, bands exist for the metallic-substrate

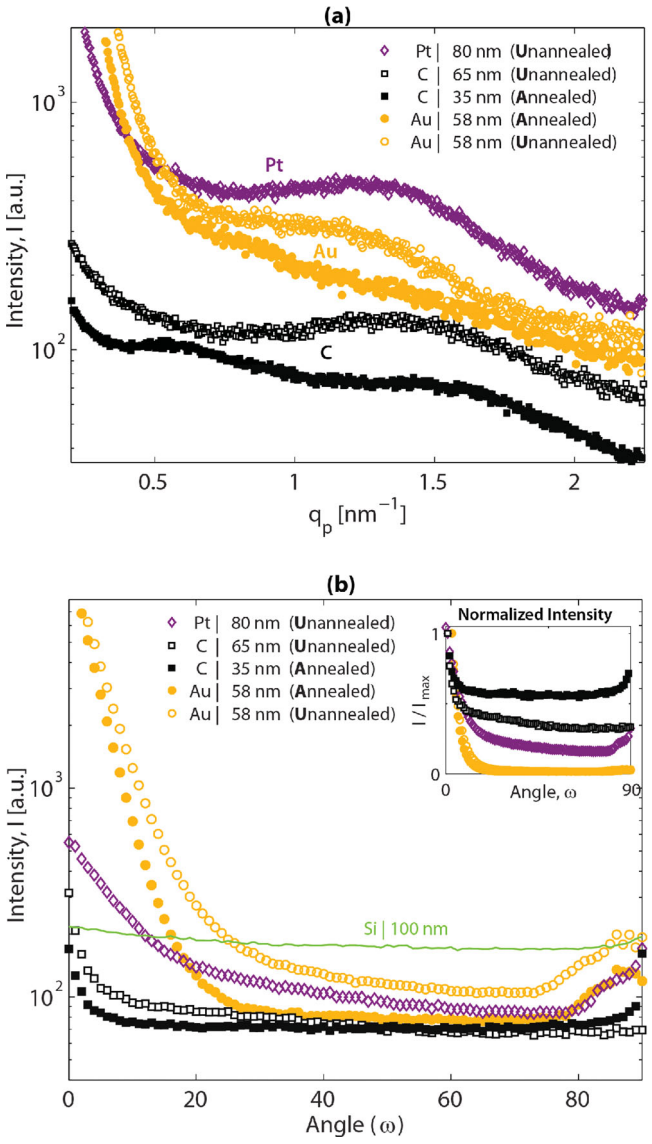

Figure 2. Line profiles for saturated Nafion thin films (100% RH): a) Along q_p (parallel to the surface) for films on Pt, Au, and C substrates. (profiles are shifted vertically for clarity). b) Orientation dependence of films plottted as intensity at the ionomer peak (shown in (a)) as a function of angle (as described in the schematics in Figure 1); the inset shows the angle-dependence for the normalized intensity. (Open and filled symbols represent unannealed and annealed films, respectively.)

samples on the bottom of the patterns at the substrate location (i.e., $q_z \approx 0.2$ to 0.3). As seen in Figure S5, Supporting Information, it is clear that these types of features occur in both unannealed and annealed samples on gold and platinum, regardless of whether the films are spin-cast and self-assembled. Similar bands at the substrate were not observed for Nafion films on carbon or silicon substrates, although the latter did exhibit some pinning of the crystallites in thin films.[34] The origin of the bands is still under investigation and may be due to the interactions of a standing wave that results on metallic substrates due to differences in refractive indices, or may be indicative of possible ordering of domains. If the latter is true, such a finding is consistent with observations in the large increase in mechanical properties,[47] low water uptake,[4] and antiplasticization behavior[37] for Nafion thin films. Overall, Figure 1 clearly shows that the morphology of the thin films, as probed by the GISAXS shape and intensity of the water-domain peaks, depends on the substrate, thereby implying that substrate/film interactions influence the structural order of Nafion.

Figure 1 also compares the morphology of both annealed and unannealed samples on gold, where annealing results in a less distinct phase-separated morphology, especially for thicker samples, although it does not have a strong effect on its anisotropy (see Figure 2b). Examining the parallel line cuts from the GISAXS images, **Figure 3**, shows that the ionic domain peak broadened and decreased in intensity with annealing. The unannealed samples had a more defined and sharper ionomer peak, suggesting a more well-defined nanostructure. However, as the films approach thicknesses of 20 nm and less, the scattering peaks were not as distinct, thereby indicating a less-ordered domain structure. Similar to the results with spin-cast films, self-assembled films also exhibited less ordering and structure upon annealing (see Figure 3 for line cuts and Figure S3, Supporting Information, for GISAXS patterns), although once again, thinner samples do not exhibit a strong scattering peak. One expects a lower amount of water uptake for annealed samples due to increased crystallinity (at least for bulk membranes)[20,32] which results in a less-defined ionomer peak. This effect is also observed in the shift of the ionomer peak to higher q values for the annealed samples.

Examination of the carbon samples in Figure 2a demonstrates that annealing seems to cause more significant changes compared to films on the other substrates (this is also apparent in 2D GISAXS images shown in Figure S4, Supporting Information). The more defined peaks for annealed films on carbon also suggest that the annealing process induces crystallinity in the samples on carbon, which may be indicative of weaker surface interactions on carbon than gold (also see Figure S6, Supporting Information). To explore this issue, **Figure 4** shows the GIWAXS profiles for annealed and unannealed spin-cast films on carbon. The impact of annealing is evident in the existence of a strong and anisotropic WAXS scattering ring indicative of crystalline order. The line profiles show that upon annealing a crystalline peak appears around $q = 12$ nm^{-1} next to the amorphous peak at 10.5 nm^{-1}. This annealing-induced crystalline order with spacing of 0.5 nm corresponds to the CF_2 chains of PTFE crystallites and has been consistently observed for bulk Nafion membranes.[15,18,20,32,48] This crystallinity can form crystallites as noted, which subsequently reduce the water uptake by increasing the backbone physical crosslinking, which is witnessed in Figure 4 by shifts in the ionomer peak around $q = 1.5$ nm^{-1}. As the films approach the crystallite sizes, the impact of annealing is expected to decrease since the chains become topologically confined at these thicknesses.

Similarly, direct comparison of the self-assembled to the spin-cast films in Figure 3 exhibits a lower q value for the spin-cast films and an apparent less broad ionomer peak. This is the same trend as was witnessed in the literature for self-assembled versus spin-cast films on silicon, albeit from different studies[8,36] and shown in Figure S6, Supporting Information. One explanation may be that the self-assembly process

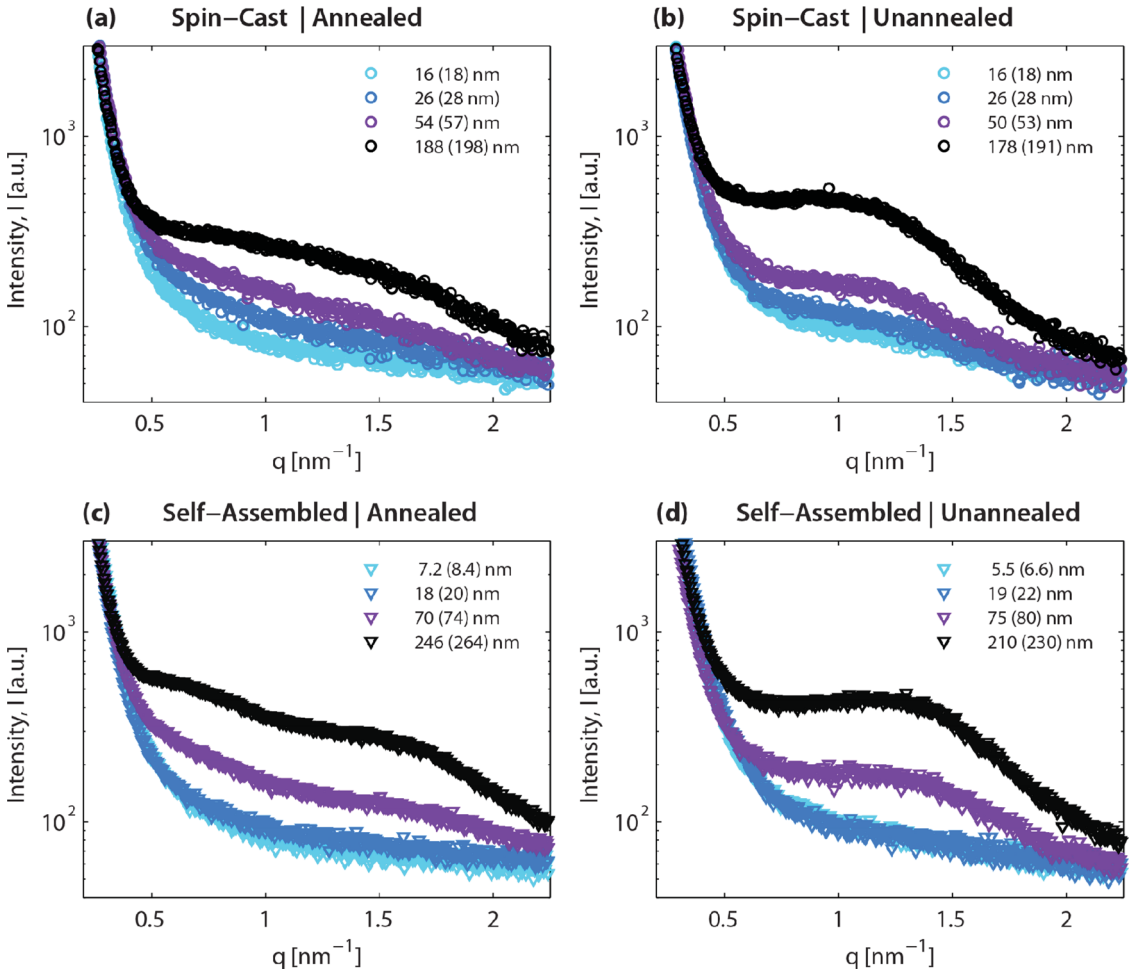

Figure 3. Line profiles along q_p for Nafion Films of varying thickness on gold showing the effect of annealing and casting method (spin-cast vs self-assembled). Thicknesses shown in the legend and in paranthesis are the nominal values (for dry films) and approximate maximum values (for hydrated films), respectively.

is governed more strongly by the interaction of dispersed colloids with the substrate surface, and since the sulfonate groups strongly interact with gold, the structure is pinned more significantly during self-assembly from solution compared to during spin-casting. This concept also seems in agreement with the more defined structure after annealing with the self-assembled films (see Figure 3 and Supporting Information Figures S2 and S3). The above idea is also in accord with the trends for Nafion films on silicon, which does not exhibit such strong specific interactions, likely due to a hydration layer at the native oxide surface. Finally, as seen in Figure 3, the self-assembled films also demonstrate a loss of phase separation below sample thicknesses of about 20 nm.

2.2. Water Uptake and Swelling

The morphology indicates that the film structure is dictated by both confinement effects as well as specific interactions with the substrate. These drivers of film structure are expected to impact the overall water content and subsequent swelling of the thin films as probed by ellipsometry and QCM. In other work, we have observed that hydrated Nafion films of less than 600 nm showed no dissipation or viscoelastic losses during measurements and their mass change could be accurately described by Sauerbrey analysis.[49] **Figure 5** shows the thickness swelling and water uptake for unannealed and annealed spin-cast and annealed self-assembled samples on gold (the complete data set is given in Tables S1–S3 in the Supporting Information). For the spin-cast unannealed samples, film thickness does not seem to impact greatly the water uptake (or the swelling) of the thin films.

The curves demonstrate the expected isotherm shape for Nafion, albeit at lower water contents than for a bulk membrane, even for some of the thicker films. This behavior is in accordance with previous work on water uptake in Nafion thin films on gold substrates.[4] Only for higher humidities, where the water uptake is driven by osmosis and not primary solvation,[38,50] do the curves deviate somewhat from each other. Similar to the morphological changes, the water uptake of the spin-cast annealed samples on gold are lower than the unannealed samples (compare Figure 5a,b with Figure 5c,d). What is apparent in the uptake data and not observed in the morphology studies is that the impact of annealing appears to be

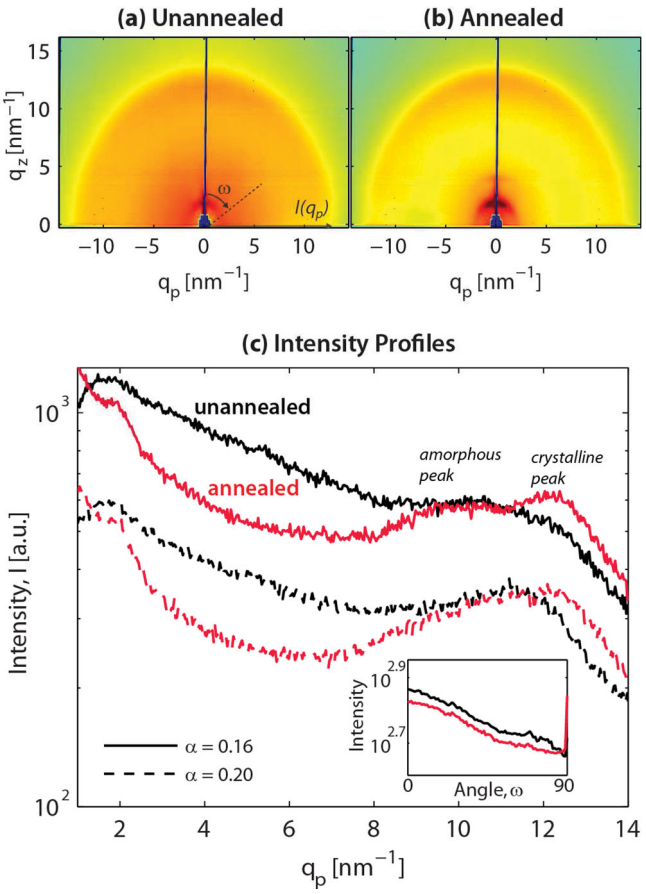

Figure 4. 2D GIWAXS patterns of a) unannealed and b) annealed Nafion film spin-cast on Carbon. c) Intensity profiles from the line cuts on 2D patterns for these samples at angles of 0.160 and 0.200. The inset shows the intensity at the WAXS peak at $\alpha = 0.16$ as a function of angle, ω, as defined in (a). Nominal thicknesses of the sample is 232 ± 17 nm.

present only for the thicker samples and not for the thinner ones. This trend is due to the more dominant substrate and confinement effects for the thinner films, which also could also be driving the changes in T_g and/or modulus with thickness and will be discussed further below.[47] This effect of thickness is especially notable at high humidity. For the self-assembled films (Figure 5e,f), the uptake is lower than that of both the bulk membrane and the spin-cast thin films. The swelling and uptake curves appear to be separated into two groups, especially at higher RH, where the thicker films exhibit very similar uptake behavior and lower water contents compared to the thinner samples. For the thinnest film, comparison of QCM and ellipsometry data deviate the most, thus suggesting that the swelling and uptake processes are more complicated than just one-dimensional or volume additivity swelling.

To explore the relationship between QCM and ellipsometry in more detail hydration numbers, λ (mol H_2O/mol SO_3^-), were calculated and compared. For most substrates, ellipsometry is a much easier technique to employ than QCM due to issues with coating QCM crystals with the various substrates and then casting before measurements. Previously, it has been shown that qualitative agreement in swelling and uptake trends between QCM and ellipsometry validated the use of ellipsometry for examining samples' relative water uptake, at least for silicon substrates.[8] Figure 5 also demonstrates a general agreement in the trend between the two techniques for most cases; however, it is worthwhile to compare them on a more quantitative basis.

QCM measures the mass uptake of a sample and ellipsometry infers the dimensional swelling change by measuring the change in the optical response of the thin film. This swelling change is dependent on parameters such as the refractive index of the material, which must be modeled for the specific conditions. For most thin-film studies, an assumption of one-dimensional swelling is employed due to the impact of confinement and the assumption of no significant excess free volume or macroscale voids.[4,37,41] To directly compare the two techniques, the hydration number, λ, is used. While hydration number or the mass % water in the film is directly determined by the gravimetric weight change in QCM, in ellipsometry λ must be calculated from the measured thickness change by using the film's swelling dimension, m (e.g., 1 for one-dimensional and 3 for three-dimensional swelling) and accounting for changes in partial molar volumes or volume of mixing, ΔV_{mix}. For the latter, it is known that at least for bulk membranes, the partial molar volumes change as a function of hydration due to the mechanism of solvation and swelling.[51]

By matching the isotherms from both measurements for nominally the same thickness, one can determine the swelling dimension using (See supporting information for details and derivations)

$$1 + \underbrace{(\lambda)}_{\text{QCM}} \frac{\bar{V}_{H_2O}}{\bar{V}_0} - \frac{\bar{V}_{mix}}{\bar{V}_0} = \frac{V_{RH}}{V_0} = \underbrace{\left(1 + \frac{\Delta L_{RH}}{L_0}\right)^m}_{\text{Ellipsometry}} \quad (1)$$

where (partial) volume of mixing $\bar{V}_{mix}$ reflects the contribution due to non-ideal mixing. Since the partial molar volumes for the thin films are unknown, the analysis was done for two cases: i) assuming ideal mixing (i.e., $\Delta V_{mix} = 0$, $\bar{V}_{mix} = 0$) to determine the unknown swelling dimension, m, and ii) assuming one-dimensional swelling ($m = 1$), which has been suggested in the literature for Nafion thin films,[36] to determine the volume of mixing ($\bar{V}_{mix}$). The results of these analyses for the data on gold (which represents all of the QCM data available) for the two cases are given in **Figure 6**, with the fits plotted in Figure S7, Supporting Information. For the assumption of ideal mixing, Figure 6a, the thinnest annealed self-assembled films demonstrate an unusual swelling dimension of less than 1 and show large deviations with thickness and thermal treatment, which may be due to the adsorption of the Nafion colloids from the solution to the gold during casting resulting in a more heterogeneous film. However, this result could also be indicative of the ideal-mixing assumption as discussed below. For most of the samples, the swelling dimension is between $m = 1$ and 2, thereby indicating that one-dimensional swelling is not necessarily the best assumption, especially for very thick films, and that some lateral swelling occurs or perhaps there are factors not accounted for in the ellipsometry thickness analysis. To further investigate the ideal-mixing conditions, Equation 1 is used but under the assumption of one-dimensional swelling (i.e., $m = 1$) so that the volume of mixing is used to match

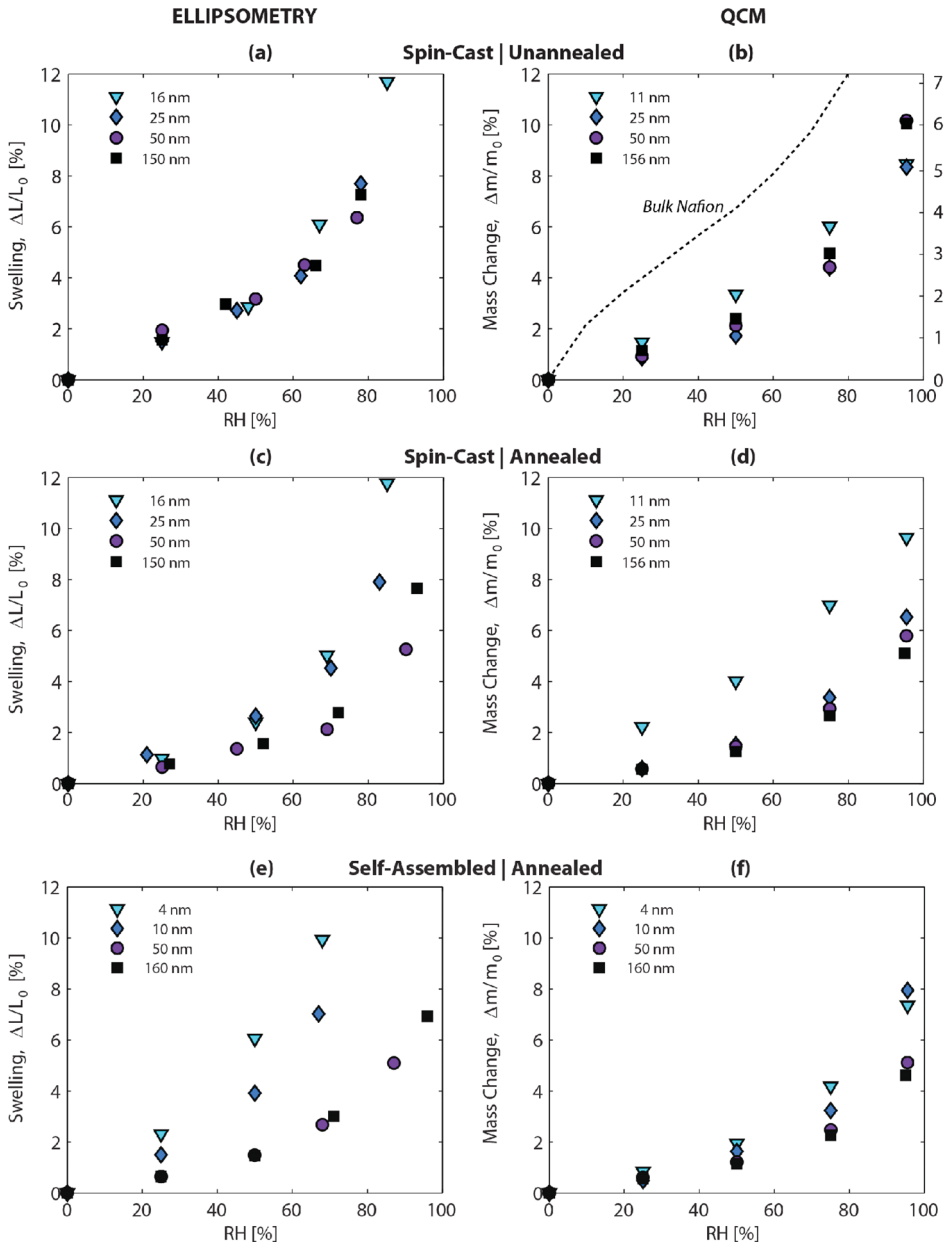

Figure 5. a,c,e) Thickness swelling from ellipsometry and b,d,f) water uptake from QCM for Nafion films on gold for a,b) spin-cast unannealed and c,d) annealed and e,f) self-assembled annealed. The data for bulk Nafion 212 membrane is shown for comparison in (b) and is found in the literature.[20]

the two data sets, Figure 6b. This analysis suggests that the volume of mixing for thin films are much lower compared to that measured for bulk PFSA membranes, with a notable exception of thick self-assembled films. Assuming two-dimensional swelling ($m = 2$) still does not provide a very good match between the volume of mixing in bulk and thin-film PFSA ionomers. This gap reflects the fact that the thin films swell even though their water content is in a range where bulk materials do not significantly change dimension. Physically, the low volume-of-mixing effect perhaps indicates that confinement effects also influence phase-separation and solvation phenomena in the polymer or there are additive free volume effects in thin films. The qualitative trends though between the QCM and ellipsometry data are consistent, and ellipsometry results are used in the remainder of the article to explore general trends and impacts of processing and substrate on film behavior.

Figure 5 allows conclusions to be drawn with respect to the impact of confinement, processing, and substrate type on uptake in terms of swelling. As noted above, the swelling of the thin films on gold demonstrates that as the thickness decreases, the water uptake decreases and then begins to increase for thicknesses of approximately 20 nm and below. The decrease in swelling for thinner films is in agreement with other studies of thin film uptake on gold substrates[4] but the subsequent increase was only measured previously with self-assembled films on silicon,[8] although other studies on gold

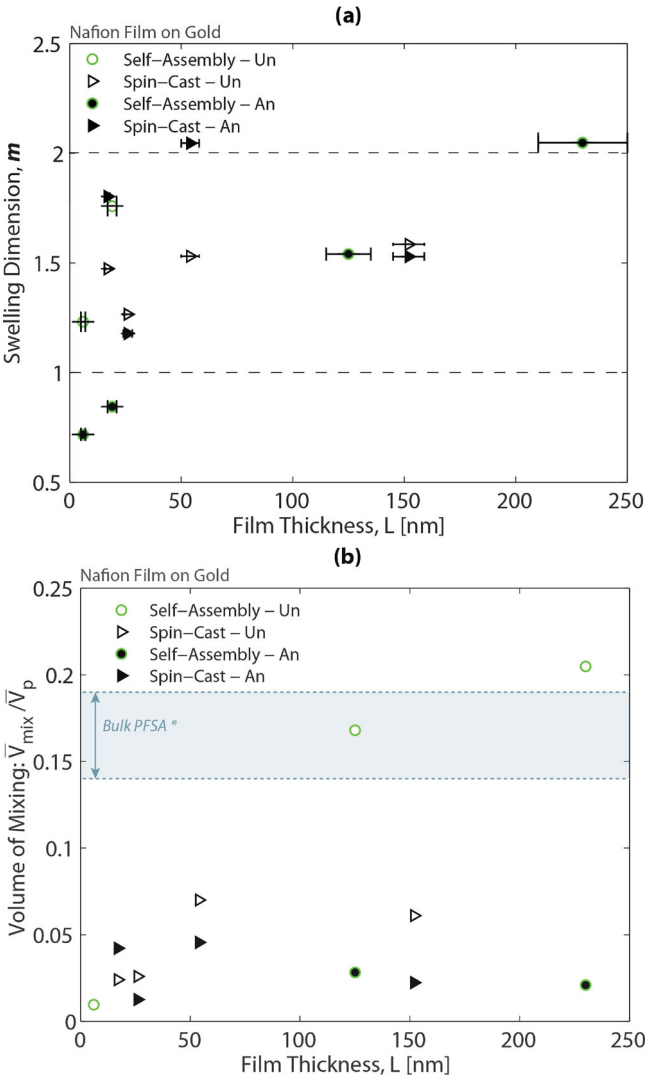

Figure 6. a) Swelling dimension, *m*, from the volume swelling (using ellipsometry) that best matches the weight change from QCM assuming zero volume of mixing ($\bar{V}_{mix} = 0$). b) Volume of mixing for a saturated film calculated from the comparison of weight change (QCM) and thickness swelling (Ellipsometry) assuming 1D swelling (i.e., $m = 1$). Range for the volume of mixing for bulk PFSA* are shown from reference [51] (See Supporting Information for details. Open and filled symbols represent unannealed and annealed films, respectively.)

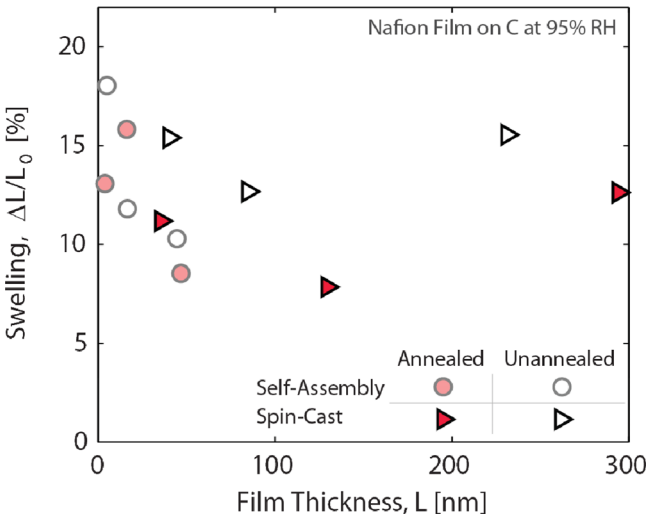

Figure 7. Variation of swelling with film thickness for Nafion films spin-cast on carbon shown at 95% RH. Bulk membrane values are estimated to be 0.12 and 0.18 from water uptake assuming a swelling dimension of 1 and 1.5, respectively, and measured as 0.14 to 0.21.[3,31]

did not probe very thin. The reason for the increase, especially at higher humidities, is the decreased phase separation in very thin films, which is observed regardless of thermal treatment and casting process. In fact, as shown in **Figure 7**, the swelling on carbon demonstrates a similar dependence on thickness with a decrease for thinner films and then an increase in swelling for the thinner samples at around 20 nm when compared with thicker samples at nominally the same humidity. These swelling values for films are lower than the swelling of bulk membranes, which was reported to be between 0.12 to 0.14 in the in-plane direction.[3,31] The swelling is also higher than on gold and silicon for spin-cast films,[4,34] but lower than that of the bulk membrane[29,31] and unannealed self-assembled thin film on silicon.[8] The impact of annealing is more evident with the samples on carbon substrates with the unannealed films demonstrating a higher water uptake, although the uptake curves with humidity are similar with deviations only at high humidity for the spin-cast annealed samples as shown in Figure S8, Supporting Information.

To explore the impacts of annealing in more detail, the difference between the swelling of annealed and unannealed samples with the same substrate and casting condition were calculated and plotted in **Figure 8** as a) function of RH for comparable thickness or b) function of thickness for comparable RH. The plots show that annealed films always have lower swelling, regardless of the substrate type and casting method, although the thinnest films on gold demonstrate no appreciable change in swelling with annealing. Moreover, the impact of annealing appears to be negligible below 60% RH as was observed in Figure 5 for thin films on gold substrates. These trends are in agreement with the less well-defined ionomer peak for the annealed samples compared to the unannealed samples, as well as the appearance of crystallite-associated peaks seen in GIWAXS ($q \approx 12$ nm^{-1}, Figure 4) and GISAXS ($q \approx 0.6$ nm^{-1}, Figure 2) of the annealed films. Surprisingly, the decrease in swelling with annealing persists on carbon substrates even for the thinner samples as shown in Figure 8b, which approach and are below the expected crystallite sizes observed in bulk samples. This data for samples on carbon substrates indicates that backbone crystallinity and alignment results in a change in mechanical properties for Nafion thin films, thus resulting in less swelling.[47] These changes increase the physical crosslinking of the polymer backbone and change the chemical/mechanical energy balance that controls the water uptake, thereby decreasing the water uptake and swelling compared to the unannealed samples.

However, as shown in Figure 8b, the trend in swelling for thin films on gold appears counter to that on the carbon substrates. In the latter case, especially for the spin-cast films, the impact of annealing decreases as the film thickness decreases

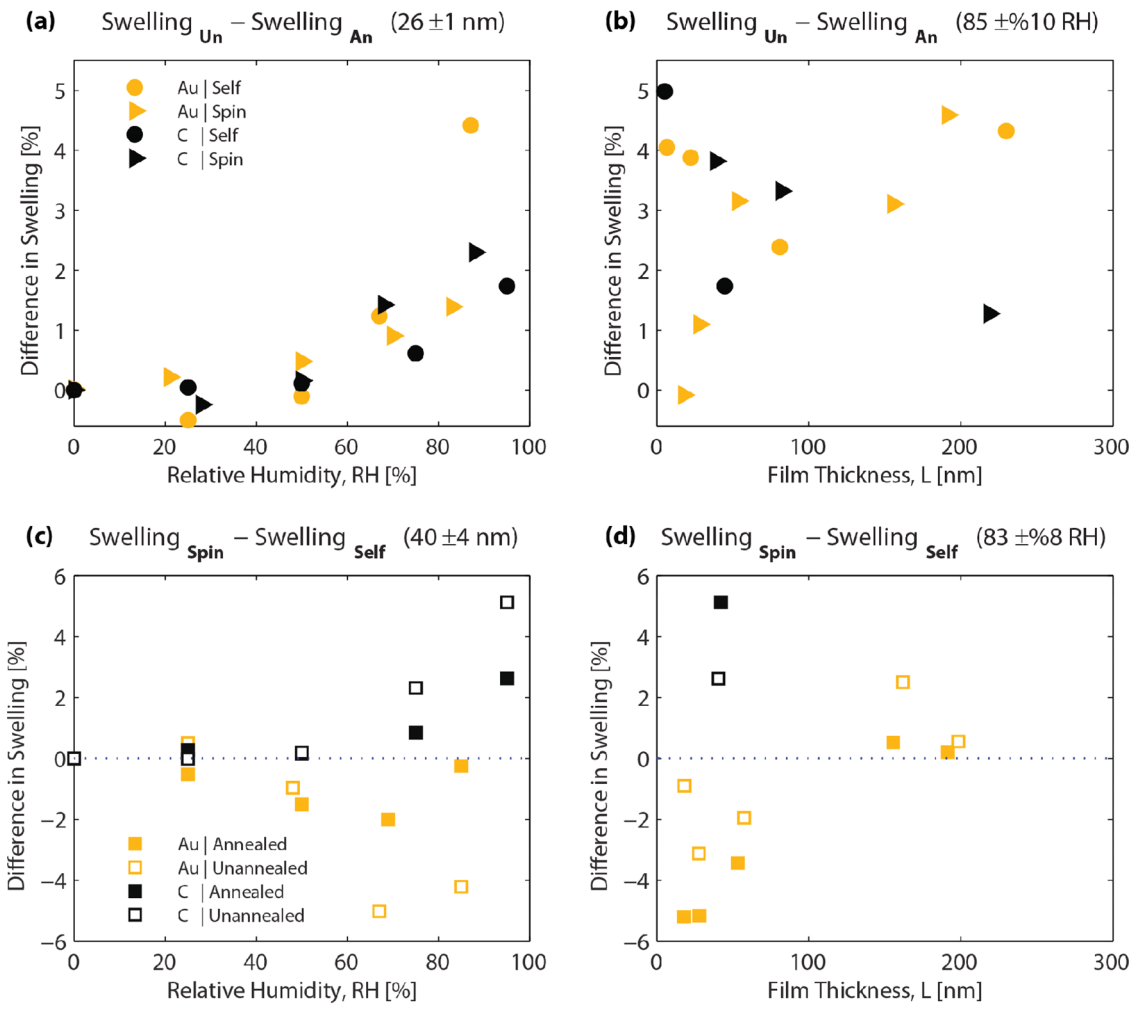

Figure 8. Difference in thickness swelling of thin films due to a,b) annealing and c,d) casting as functions of a,c) varying humidity for a given thickness and b,d) varying thickness for a given humidity on gold and carbon substrates.

on gold, although when occurring, annealing always decreases the swelling response. The annealing-driven decrease in swelling of self-assembled films demonstrated relatively weaker dependence on thickness, and this different behavior compared to spin-cast samples may be due to the method of film formation resulting in less strong specific interactions between the polymer and the gold substrate. For the thicker films, the impact of annealing is greater for films on gold than for films on carbon owing to the combined effects of possible specific sulfonate surface interactions with gold and the stronger changes in thicker films due to annealing, where the results are somewhat similar to the annealing effect witnessed on hydrophobized silicon substrate versus a hydrophilic silicon native oxide surface.[34] Thus, the decrease in the impact of annealing with thickness on gold is seemingly explained by increased surface interactions that dominate over the thermal treatment changes as the films become thinner, where these interactions are not as strong for Nafion on carbon and silicon substrates. Thus, the thinner films on gold are possibly pinned to the surface and cannot re-arrange under the thermal conditions used in this work which is supported by no observable change in the GISAXS patterns of these samples with annealing (see Figure 1). Thus, the impact of annealing on the morphology and mechanical properties of the films is rather limited for thinner films, and similar uptake as unannealed samples is observed.

Similar to the annealing comparison, the impact of the casting procedure is shown in Figure 8c,d by plotting the swelling difference between self-assembled and spin-cast films. Analogous to the annealing studies, an influence of film processing is not observed below 60% RH, where the uptake is driven by primary solvation of the sulfonate groups. As Figure 8d and comparisons of Figure 5c,d with Figure 5e,f show, the swelling and presumed water uptake in the self-assembled films is greater than for the spin-cast samples on gold. This difference increases with decreasing thickness for both annealed and unannealed films. The higher water content is the same trend as seen on silicon, where self-assembled Nafion films between 4 and 50 nm demonstrated an enhanced water uptake[8] compared to spin-cast samples.[34,36] An interesting finding is that, compared to spin-cast films, swelling of self-assembled films is lower on carbon, especially for higher humidities for the ≈40 nm samples.

2.3. Swelling Kinetics

The discussion above focuses on the quasi-equilibrium water uptake, swelling, and morphology of thin films. It is also instructive to examine the kinetics of swelling. Ellipsometry results for the swelling of films as a function of time during humidification from 0 to 100% RH are shown in **Figure 9**a for samples on gold substrates. Similar qualitative trends and even swelling fractions are observed for films on carbon (see Figure S8, Supporting Information), which are also in agreement with previously published results on silicon[34] and gold.[4] Films reach 50% of their quasi-equilibrium value in a few minutes and approach steady-state in 15 to 25 min, regardless of the substrate. A slow, continuous increase in swelling was observed for all Nafion thin films, a phenomenon commonly observed for bulk Nafion ionomers even at larger timescales (up to days) and attributed to the long-term relaxation of the polymer matrix leading to additional water uptake.[27,29,30,52]

For a more quantitative comparison, time constants determined from double-exponential fitting of the ellipsometry data,

$$\frac{L(t)-L_0}{L(t_\infty)-L_0} = 1 - A\exp\left(-\frac{t}{\tau_1}\right) - (1-A)\exp\left(-\frac{t}{\tau_2}\right) \quad (2)$$

are shown in Figure 9b as a function of hydrated film thickness (see Supporting Information for calculations). The time constants for samples on gold are smaller than those for samples on carbon and annealing impacts the behavior of samples on carbon more so than samples on gold. These observations are in agreement with gold having stronger interactions with the Nafion thin films and the films on carbon substrates being impacted more so by annealing due to weaker polymer-carbon interactions. Interestingly, there is not a strong dependence between thickness and the time constant, thereby indicating that transport through the film is not limiting and the swelling is likely driven by polymer relaxation or water partitioning into the film.

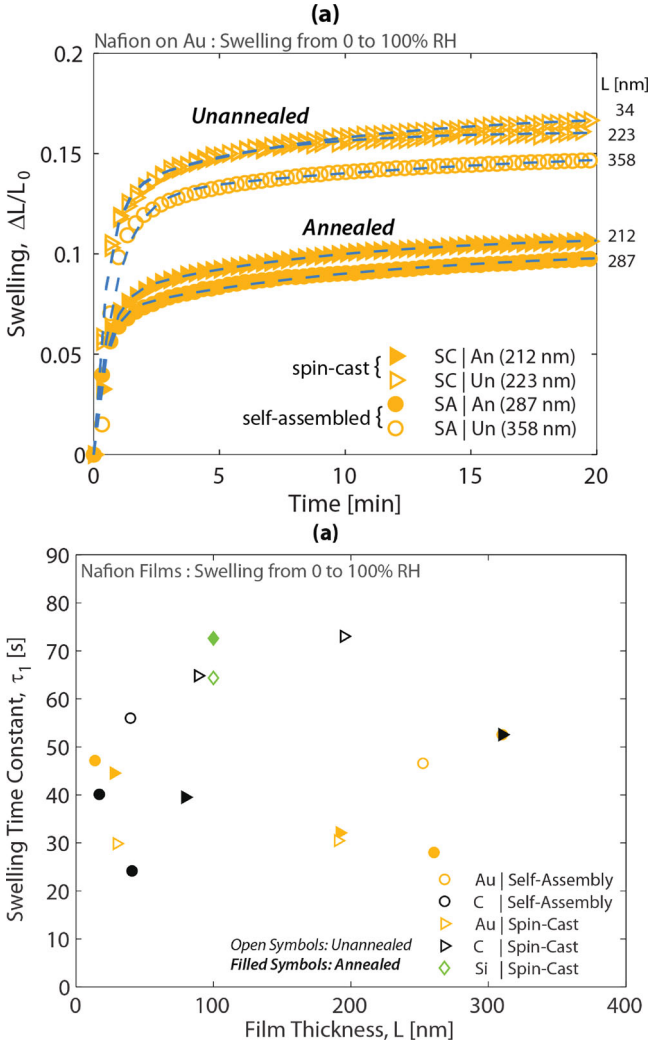

Figure 9. a) Time-dependent ellipsometry from 0% to 100% RH, and b) swelling time constant (τ_1) as a function of maximum (final) thickness (i.e., $L(t_\infty)$ in Equation (2) as determined from 0 to 100 % RH time-dependent ellipsometry. (Open and filled symbols represent unanneald and annealed films, respectively.)

3. Summary

In this article, the impacts of various processing conditions including casting method, annealing, and thickness on Nafion thin-film morphology and water uptake and swelling on various substrates was investigated. The findings demonstrate a complex interplay between the perfluorosulfonic-acid ionomer and the various substrates, where different anisotropies and possibly structures are witnessed. Lower water uptake is observed where annealing impacts other substrates (carbon in this study and silicon from the literature) more significantly than the metallic ones, especially for thicker samples. These effects are observed at higher humidities, where low humidities are dominated by primary sulfonate group solvation and thus do not show strong differences in water uptake or swelling. Quantitative analysis of swelling kinetics and comparisons between water uptake by quartz-crystal microbalance and swelling by ellipsometry show that the swelling appears to be greater than one-dimensional or demonstrate much lower than expected volume of mixing effects as compared to bulk ionomers. Self-assembled and spin-cast films demonstrated different behavior depending on the substrate, typically with unannealed self-assembled films showing the greatest water swelling except on carbon. For all of the films, a transition region between ≈20 to 100 nm was observed where the water content and associated swelling decreased from the bulk membrane value, but then increased for films below approximately 20 nm. The morphology likewise showed a lower degree of phase separation for the thinnest films, suggesting that their mechanical properties are no longer sufficient to limit the hydration or solvation energies due to lack of crystallite formation. The specific surface interactions and the confinement effects result in complex responses that alter the underlying chemical/mechanical energy balance governing water uptake and swelling of the films. The results shown here are important for understanding transport and uptake in these materials, especially when existing as thin films in fuel-cell catalyst layers and related porous electrodes in

electrochemical devices as well as serving as interesting systems to understand the underlying ionomer polymer physics.

4. Experimental Section

Materials: For ellipsometry and GISAXS studies, silicon wafer substrates with gold, platinum, and carbon surfaces were fabricated. The silicon wafers (SVMI, Santa Clara, CA) were prepared using a 1:3 (30% H_2O_2:sulfuric acid) piranha solution for 20 min and then washed with deionized water. For gold, chromium was used as an adhesion layer on the silicon wafer. During thermal evaporation, chromium was baked out for 30 min and gold was baked out for 60 min before deposition for contaminant removal. The thermal evaporation process took place with a base pressure of 7×10^{-7} Torr at a rate of 3 Å s^{-1} until a thickness of 20 nm and 50 nm was achieved for chromium and gold, respectively. For carbon substrates, a polyfurfuryl alcohol/acetone solution was spun coated unto a silicon wafer and then dried at 40 °C under vacuum for 15 min. The pyrolysis of the polyfurfuryl alcohol to carbon was carried out using a process developed by Lee et al.[53] where the polymer-coated silicon wafers were heat-treated in a quartz tube furnace under vacuum with Argon flow. The temperature was ramped at 2 °C min^{-1} to 350 °C and held constant for 4 h, followed by a 1 °C min^{-1} ramp to 500 °C with a constant hold for 4 h to allow time for pyrolysis. Then, the temperature was ramped at 5 °C min^{-1} to 800 °C followed by a 2 h isothermal hold. The samples were then cooled at 2 °C min^{-1} to room temperature. Figure S10, Supporting Information, shows that the amount of PFA did not change the profiles and also that the substrate itself did not hydrate under the humidities chosen. For QCM, gold-electrode 5 MHz quartz crystals (Inificon, East Syracuse, New York)) were employed as substrates.

Thin-Film Preparation: Nafion (EW 1100) solution (5 wt%) in water-alcohol mixture (75/20 w/w alcohol to water) obtained from Ion Power (USA) was used as the stock Nafion solution. Self-assembled thin films of Nafion were fabricated following the procedure developed by Karan and coworkers.[41,42,54] The stock Nafion solution was diluted to desired concentrations of 0.1, 0.25, 1, and 3 wt% by addition of isopropyl alcohol (IPA) (Sigma Aldrich). The diluted solutions were sonicated for 5 min and equilibrated for at least 24 h. Nafion concentrations were chosen based on the findings of Paul et al.[41], who determined that the corresponding thickness of self-assembled films to be about 4, 10, 55, and 160 nm, respectively. For fabrication of Nafion thin films, the substrates were immersed in diluted Nafion solution for 12 h to allow self-assembly. Subsequently, after carefully removing the substrate from the solution it was dried under a flow of dry air. For preparation of Nafion films on gold for QCM, the crystal was placed into the QCM holder and the loaded QCM holder was immersed in the requisite Nafion solution and dried as described above. Spin-cast films were fabricated by diluting stock Nafion solution to concentrations of 0.5, 1, 2, and 5 wt% by addition of IPA. The diluted solutions were given 24 h to equilibrate. Films were prepared by dropping 15 µL of solution on a substrate at rest and then the sample was immediately spun at 3000 rpm and one 5 wt% sample at 2000 rpm until dry by sight. After the rotation returned to rest, the samples were then placed under flowing dry air for further drying, followed by vacuum drying at 40 °C for 16 h. The same procedure was used for both the silicon wafer substrates and the QCM substrates. For both preparation methods, films were either left unannealed as prepared or annealed at 146 °C for 60 min.

Water-Uptake Measurements: As described previously, water uptake was measured both by ellipsometry as well as QCM for select samples.[8] Film thicknesses were measured in situ under varying relative humidity (RH) using a J.A. Woollam RC2-XI dual rotating compensator multichannel spectroscopic ellipsometer. The change in the wave amplitude (Ψ) and phase shift (Δ) was measured over a spectral range of 240 to 1700 nm (0.75–5.15 eV). Once Ψ and Δ were characterized as a function of photon energy, a Lorentz oscillator-based materials model was used to derive the thickness and optical properties of the polymer films on optically characterized substrates. The change in thickness and complex refractive index were calculated for films exposed to 0, 25, 50, 75, and 90 % RH in an in-house constructed environmental cell held at ambient temperature. The cell was made with non-polarizing fused silica windows to maximize the amount of light transmitted. Water uptake for the gold samples was also measured using a QCM (Maxtek/Inficon, East Syracuse, NY) and Saurbrey analysis. The entire QCM holder was enclosed in a poly(ethyelene) in-house constructed humidity chamber maintained at ambient temperature. For humidification in both ellipsometry and QCM experiments, air at dewpoint was produced using a sparging system. The humidified wet air was mixed with a stream of dry air and the flow rates of the wet and dry streams were varied using electronic mass-flow controllers (Omega FMA5512, Omega Engineering, Inc., Stamford, CT) to achieve a specific relative humidity at ambient pressure. An RH probe (Omega HX15-W) was connected to the gas outlet from the ellipsometry or QCM in-house constructed humidity chambers for in-situ monitoring of the relative humidity of the sample environment.

Grazing-Incidence Small-Angle X-Ray Scattering (GISAXS) Measurements: GISAXS measurements were performed as described previously in the literature.[34] Thin-film samples were placed into an in-house built environmental chamber with X-ray transparent Kapton windows. The sample was equilibrated at 100% RH at room temperature (22 °C) and GISAXS patterns were collected as a function of time for at least 45 mins, after which the sample was assumed to be saturated with water vapor. All the GISAXS patterns presented here were collected at an incidence angle (α) above the critical angle for Nafion but below that for the substrate, which was generally around $\alpha = 0.2$ degrees, but varied within the range of 0.15 to 0.26 due to the variations among the substrates. GIWAXS experiments were conducted in ambient conditions for Nafion samples on carbon with the incidence angles between 0.16 and 0.22. All X-ray scattering experiments were performed in beamline 7.3.3 of the Advanced Light Source (ALS) at Lawrence Berkeley National Laboratory (LBNL). Sample to detector distance was approximately 1.8 m and 25 cm for the GISAXS and GIWAXS configurations, respectively. Exposure time for the collected images was 20 s. The X-ray energy used was 10 keV, with a monochromator energy resolution E/dE of 100, and the patterns shown were acquired with a 2D Dectris Pilatus 1M CCD detector (172 µm × 172 µm pixel size).

Supporting Information

Supporting Information is available from the Wiley Online Library or from the author.

Acknowledgements

The authors thank Dr. Miguel Modestino for helpful discussions and preparation of the Pt substrates. The authors also thank Dr. Alex Hexemer for helpful discussions and facilitating the use of equipment at the Advanced Light Source (ALS) in Berkeley Lab. A.K. and A.Z.W. were supported by the Assistant Secretary for Energy Efficiency and Renewable Energy, Fuel Cell Technologies Office, of the U. S. Department of Energy under contract number DE-AC02-05CH11231; D.K. and M.A.H. acknowledge the support of the U.S. Department of Energy, the Office of Energy Efficiency and Renewable Energy, Fuel Cell Technologies Office through a subcontract from General Motors Corporation under Grant DE-EE0000470; D.K.P. and K.K. acknowledge financial support from Natural Sciences and Engineering Research Council of Canada (NSERC). This work made use of facilities at the Advanced Light Source (ALS) beamline 7.3.3, supported by the Office of Science, Office of Basic Energy Sciences, of the U.S. Department of Energy (Contract No. DE-AC02-05CH11231).

Received: December 30, 2013
Revised: February 20, 2014
Published online: April 24, 2014

[1] a) A. Z. Weber, M. M. Mench, J. P. Meyers, P. N. Ross, J. T. Gostick, Q. H. Liu, *J. Appl. Electrochem.* **2011**, *41*, 1137; b) M. S. Dresselhaus, G. W. Crabtree, M. V. Buchanan, *MRS Bull.* **2005**, *30*, 518; c) G. Inzelt, M. Pineri, J. W. Schultze, M. A. Vorotyntsev, *Electrochim. Acta* **2000**, *45*, 2403.
[2] a) P. W. Majsztrik, M. B. Satterfield, A. B. Bocarsly, J. B. Benziger, *J. Membrane Sci.* **2007**, *301*, 93; b) B. Kienitz, H. Yamada, N. Nonoyama, A. Z. Weber, *J. Fuel Cell Sci. Technol.* **2011**, *8*, 011013.
[3] Q. Zhao, P. Majsztrik, J. Benziger, *J. Phys. Chem. B* **2011**, *115*, 2717.
[4] A. Kongkanand, *J. Phys. Chem. C* **2011**, *115*, 11318.
[5] a) J. M. Spurgeon, M. G. Walter, J. F. Zhou, P. A. Kohl, N. S. Lewis, *Energy Environ. Sci.* **2011**, *4*, 1772; b) J. M. Spurgeon, N. S. Lewis, *Energy Environ. Sci.* **2011**, *4*, 2993.
[6] a) R. Makharia, M. F. Mathias, D. R. Baker, *J. Electrochem. Soc.* **2005**, *152*, A970; b) T. Mashio, K. Malek, M. Eikerling, A. Ohma, H. Kanesaka, K. Shinohara, *J. Phys. Chem. C* **2010**, *114*, 13739; c) Z. Xie, T. Navessin, K. Shi, R. Chow, Q. P. Wang, D. T. Song, B. Andreaus, M. Eikerling, Z. S. Liu, S. Holdcroft, *J. Electrochem. Soc.* **2005**, *152*, A1171.
[7] a) Z. Siroma, T. Ioroi, N. Fujiwara, K. Yasuda, *Electrochem. Commun.* **2002**, *4*, 143; b) S. A. Eastman, S. Kim, K. A. Page, B. W. Rowe, S. Kang, C. L. Soles, K. G. Yager, *Macromolecules* **2012**, *45*, 7920.
[8] M. A. Modestino, D. K. Paul, S. Dishari, S. A. Petrina, F. I. Allen, M. A. Hickner, K. Karan, R. A. Segalman, A. Z. Weber, *Macromolecules* **2013**, *46*, 867.
[9] A. Kusoglu, A. Kwong, K. T. Clark, H. P. Gunterman, A. Z. Weber, *J. Electrochem. Soc.* **2012**, *159*, F530.
[10] a) J. Peron, D. Edwards, M. Haldane, X. Y. Luo, Y. M. Zhang, S. Holdcroft, Z. Q. Shi, *J. Power Sources* **2011**, *196*, 179; b) T. Soboleva, K. Malek, Z. Xie, T. Navessin, S. Holdcroft, *ACS Appl. Mater. Interfaces* **2011**, *3*, 1827; c) H. Iden, K. Sato, A. Ohma, K. Shinohara, *J. Electrochem. Soc.* **2011**, *158*, B987.
[11] K. A. Mauritz, R. B. Moore, *Chem. Rev.* **2004**, *104*, 4535.
[12] M. A. Hickner, B. S. Pivovar, *Fuel Cells* **2005**, *5*, 213.
[13] M. A. Hickner, *J. Polym. Sci.: Pol. Phys.* **2012**, *50*, 9.
[14] M. Eikerling, A. A. Kornyshev, A. R. Kucernak, *Phys. Today* **2006**, *59*, 38.
[15] G. Gebel, O. Diat, *Fuel Cells* **2005**, *5*, 261.
[16] G. Gebel, *Polymer* **2000**, *41*, 5829.
[17] M. H. Kim, C. J. Glinka, S. A. Grot, W. G. Grot, *Macromolecules* **2006**, *39*, 4775.
[18] T. D. Gierke, G. E. Munn, F. C. Wilson, *J. Polym. Sci., Polym. Phys.* **1981**, *19*, 1687.
[19] L. Rubatat, A. L. Rollet, G. Gebel, O. Diat, *Macromolecules* **2002**, *35*, 4050.
[20] A. Kusoglu, S. Savagatrup, K. T. Clark, A. Z. Weber, *Macromolecules* **2012**, *45*, 7467.
[21] M. Bass, A. Berman, A. Singh, O. Konovalov, V. Freger, *J. Phys. Chem. B* **2010**, *114*, 3784.
[22] Q. He, A. Kusoglu, I. T. Lucas, K. Clark, A. Z. Weber, R. Kostecki, *J. Phys. Chem. B* **2011**, *115*, 11650.
[23] a) P. J. James, J. A. Elliott, T. J. McMaster, J. M. Newton, A. M. S. Elliott, S. Hanna, M. J. Miles, *J. Mater. Sci.* **2000**, *35*, 5111; b) C. Wang, V. Krishnan, D. Wu, R. Bledsoe, S. J. Paddison, G. Duscher, *J. Mater. Chem. A* **2013**, *1*, 938.
[24] K. Schmidt-Rohr, Q. Chen, *Nat. Mater.* **2008**, *7*, 75.
[25] L. M. Onishi, J. M. Prausnitz, J. Newman, *J. Phys. Chem. B* **2007**, *111*, 10166.
[26] T. A. Zawodzinski, C. Derouin, S. Radzinski, R. J. Sherman, V. T. Smith, T. E. Springer, S. Gottesfeld, *J. Electrochem. Soc.* **1993**, *140*, 1041.
[27] A. Kusoglu, M. A. Modestino, A. Hexemer, R. A. Segalman, A. Z. Weber, *ACS Macro Lett.* **2012**, *1*, 33.
[28] A. Z. Weber, J. Newman, *J. Electrochem. Soc.* **2004**, *151*, A311.
[29] A. Kusoglu, A. Z. Weber, in *Polymers for Energy Storage and Delivery: Polyelectrolytes for Batteries and Fuel Cells*, ACS Symposium Series*1096*, American Chemical Society,Washington, DC **2012**, 175.
[30] L. Onishi, in *Ph.D. dissertation*, University of California, Berkeley, CA **2009**, 212.
[31] J. Peron, A. Mani, X. S. Zhao, D. Edwards, M. Adachi, T. Soboleva, Z. Q. Shi, Z. Xie, T. Navessin, S. Holdcroft, *J. Membrane Sci.* **2010**, *356*, 44.
[32] G. M. Divoux, K. A. Finlay, J. K. Park, J.-M. Song, B. Yan, M. Zhang, D. A. Dillard, R. B. Moore, *ECS Trans.* **2011**, *41*, 87.
[33] a) J. N. L. Albert, T. H. Epps Iii, *Mater. Today* **2010**, *13*, 24; b) R. A. Segalman, *Mater. Sci. Eng.: R: Rep.* **2005**, *48*, 191; c) M. J. Fasolka, A. M. Mayes, *Ann. Rev. Mater. Res.* **2001**, *31*, 323; d) T. P. Russell, P. Lambooy, G. J. Kellogg, A. M. Mayes, *Phys. B* **1995**, *213*, 22; e) E. Huang, T. P. Russell, C. Harrison, P. M. Chaikin, R. A. Register, C. J. Hawker, J. Mays, *Macromolecules* **1998**, *31*, 7641; f) P. Mansky, T. P. Russell, C. J. Hawker, M. Pitsikalis, J. Mays, *Macromolecules* **1997**, *30*, 6810.
[34] M. A. Modestino, A. Kusoglu, A. Hexemer, A. Z. Weber, R. A. Segalman, *Macromolecules* **2012**, *45*, 4681.
[35] M. Bass, A. Berman, A. Singh, O. Konovalov, V. Freger, *Macromolecules* **2011**, *44*, 2893.
[36] S. A. Eastman, S. Kim, K. A. Page, B. W. Rowe, S. H. Kang, S. C. DeCaluwe, J. A. Dura, C. L. Soles, K. G. Yager, *Macromolecules* **2012**, *45*, 7920.
[37] S. K. Dishari, M. A. Hickner, *ACS Macro Lett.* **2012**, *1*, 291.
[38] V. Freger, *J.Phys. Chem. B* **2009**, *113*, 24.
[39] P. Bertoncello, I. Ciani, F. Li, P. R. Unwin, *Langmuir* **2006**, *22*, 10380.
[40] Z. Siroma, R. Kakitsubo, N. Fujiwara, T. Ioroi, S. I. Yamazaki, K. Yasuda, *J. Power Sources* **2009**, *189*, 994.
[41] D. K. Paul, A. Fraser, K. Karan, *Electrochem. Commun.* **2011**, *13*, 774.
[42] D. K. Paul, K. Karan, A. Docoslis, J. B. Giorgi, J. Pearce, *Macromolecules* **2013**, *46*, 3461.
[43] J. A. Dura, V. S. Murthi, M. Hartman, S. K. Satija, C. F. Majkrzak, *Macromolecules* **2009**, *42*, 4769.
[44] a) B. Loppinet, G. Gebel, *Langmuir* **1998**, *14*, 1977; b) L. D. Spiro, *J. Gerontol. Nursing* **1978**, *4*, 28; c) B. Loppinet, G. Gebel, C. E. Williams, *J. Phys. Chem. B* **1997**, *101*, 1884.
[45] T. Soboleva, X. S. Zhao, K. Mallek, Z. Xie, T. Navessin, S. Holdcroft, *ACS Appl. Mater. Interfaces* **2010**, *2*, 375.
[46] a) R. Subbaraman, D. Strmcnik, V. Stamenkovic, N. M. Markovic, *J. Phys. Chem. C* **2010**, *114*, 8414; b) C. D. Bain, G. M. Whitesides, *Science* **1988**, *240*, 62; c) R. G. Nuzzo, D. L. Allara, *J. Am. Chem. Soc.* **1983**, *105*, 4481; d) C. D. Bain, E. B. Troughton, Y. T. Tao, J. Evall, G. M. Whitesides, R. G. Nuzzo, *J. Am. Chem. Soc.* **1989**, *111*, 321.
[47] K. A. Page, A. Kusoglu, C. M. Stafford, S. Kim, R. J. Kline, A. Z. Weber, unpublished.
[48] M. Fujimura, T. Hashimoto, H. Kawai, *Macromolecules* **1981**, *14*, 1309.
[49] S. Petrina, J. Torrey, L. Greenlee, N. Podraza, M. A. Hickner, unpublished.
[50] K.-D. Kreuer, *Solid State Ionics* **2012**, *252*, 93.
[51] T. A. Zawodzinski, S. Che-Nan, M. Bright, H. Ghassemi, V. DiNoto, T. Fujiwara, M. Maalouf, Y. Bai, Interrelating Physical, Thermodynamic, Structural and Funtional Properties of Proton Conducting Membranes, presented at *Water Phenomena in PEM: Sorption, Swelling and Breakthrough Processes*, Trondheim, Norway **2013**.
[52] D. T. Hallinan, M. G. De Angelis, M. G. Baschetti, G. C. Sarti, Y. A. Elabd, *Macromolecules* **2010**, *43*, 4667.
[53] H. Lee, R. Rajagopalan, J. Robinson, C. G. Pantano, *ACS Appl. Mater. Interfaces* **2009**, *1*, 927.
[54] D. K. Paul, A. Fraser, J. Pearce, K. Karan, *ECS Transactions* **2011**, *41*, 1393.